# Separated Coil and Chain Aggregation Behaviors on the Miscibility and Helical Peptide Secondary Structure of Poly(tyrosine) with Poly(4-vinylpyridine)

Yi-Syuan Lu, Yung-Chih Lin, and Shiao-Wei Kuo*

Department of Materials and Optoelectronic Science, Center for Nanoscience and Nanotechnology, National Sun Yat-Sen University, Kaohsiung, Taiwan

ABSTRACT: In this study, we synthesized a low-molecular-weight polytyrosine (PTyr) through living ring-opening polymerization of the α-amino acid-*N*-carboxyanhydride and then blended it with poly(4-vinylpyridine) (P4VP) homopolymer in *N,N*-dimethylformamide (DMF) and MeOH solutions, thereby controlling the miscibility behavior and secondary structures of the PTyr. Infrared spectroscopy revealed that the PTyr/P4VP mixture featured strong hydrogen bonds between the OH groups of PTyr and the pyridyl groups of P4VP. Differential scanning calorimetry revealed that the glass transition temperatures of the PTyr/P4VP complexes formed from MeOH solutions were higher than those of the corresponding PTyr/P4VP miscible blends obtained from DMF solutions. The behavior of the PTyr/P4VP blends obtained after evaporation of the DMF solutions was consistent with separated random coils of the PTyr chains. The increased degree of hydrogen bonding within the PTyr/P4VP complexes formed from MeOH solutions resulted in interpolymer complex aggregates; the corresponding enhanced intermolecular hydrogen bonding of PTyr with P4VP resulted in β-sheet conformations for PTyr, as evidenced from Fourier transform infrared spectroscopy, solid state nuclear magnetic resonance spectroscopy, and wide-angle X-ray diffraction analyses. This model, which takes advantage of the well-defined secondary structures (α-helices, β-sheets) of PTyr, can, therefore, be used to identity the behavior of separated coils and aggregated chains in polymer blend and complex systems.
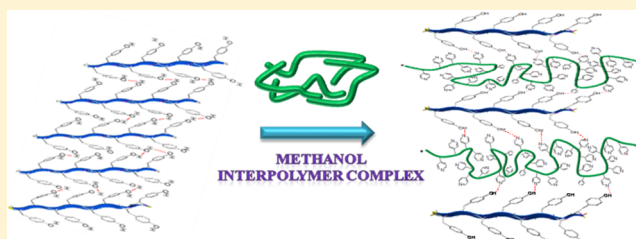
INTRODUCTION

Amino acid-based polymers, including polypeptides, have been studied widely because of their potential applications as biocompatible materials with useful chemical properties and functions that derive from the amino acid moieties.[1,2] Modification of a polypeptide with a functional polymer, such as poly(ethylene glycol) (PEG), is used typically for the development of new materials.[3–5] In addition, multiblock copolymers have also been prepared to model silk-based materials, which formed nanostructures through β-sheet self-assembly.[6] Most poly(peptide-*b*-nonpeptide) (rod/coil) block copolymers have been studied for their potential applications in tissue engineering and drug delivery.[7–21] The synthesis of diblock copolymers is, however, a difficult and time-consuming means of modifying polypeptides. From both practical and economic points of view, polymer blending of existing polymers is a more effective and convenient route toward creating new and useful materials exhibiting greater versatility and flexibility than is the development of new polypeptides.[22–27]

Polypeptides can form hierarchically ordered structures containing fundamental secondary motifs: α-helices, which can be regarded as rigid rods stabilized through intramolecular hydrogen bonding interactions, and β-sheets, stabilized by intermolecular interactions.[28] From a synthetic point of view, the α-helical structures of polypeptides cause them to behave as rigid rod-like polymers in solution and in solid states. From a

biological point of view, β-sheet secondary structures have emerged as important features in the development of several neurodegenerative disorders (e.g., prion diseases).[29] As a result, conformational studies of model polypeptides are important steps toward mimicking the biological activity of more-complex proteins.[30] In previous studies,[31,32] we found that the secondary structures of the polypeptides poly(r-methyl L-glutamate) (PMLG), poly(r-ethyl L-glutamate) (PELG), and poly(r-benzyl L-glutamate) (PBLG) could be altered through blending with other random-coil nonpeptide oligomers [namely, phenolic resin or poly(vinylphenol) (PVPh)], mediated by hydrogen bonding interactions. The content of α-helical conformations in these blend systems correlated strongly with the strengths of intermolecular hydrogen bonding to the hydrogen-bond-donor polymers. Nevertheless, these poly(L-glutamate)s formed only relatively weak intermolecular hydrogen bonds between their side chain C=O groups and the OH groups of phenolic resin or PVPh. The strongest interassociation equilibrium constant (K_A), a relatively low value of only 50, was found in the phenolic/PELG blend system, consistent with C=O groups in polymers being relatively weak hydrogen bond acceptor groups

$[K_A < K_B$ (self-association equilibrium constant) in most cases].[31]

Random coil nonpeptide polymers blended with OH-containing polymers [e.g., PVPh] with poly(4-vinylpyridine) (P4VP) are typically strongly hydrogen-bonding blend systems (in this case, K_A = 1200) and have been investigated widely.[33−38] In this study, we choose polytyrosine (PTyr) as our hydrogen-bond-donor polypeptide and blended it with P4VP to investigate the influence of their strong hydrogen bonds on the secondary structure of the peptide and their miscibility behavior. In PVPh/P4VP systems, the solvent has a dramatic effect on complex formation.[39,40] For example, a mixture of PVPh/P4VP yields a precipitated complex in low-polarity solvents (e.g., MeOH, EtOH) that exhibits a single glass transition temperature (T_g) of 210 °C that is significantly higher than that of each component of the blend (ca. 150 °C).[39,40] In contrast, no precipitation occurs in N,N-dimethylformamide (DMF) because this polar solvent also participates in hydrogen bonding and competes with P4VP for the OH groups of PVPh. Because DMF is a much stronger hydrogen bond acceptor than MeOH, it does not allow the formation of the interpolymer complex.[41] The polymer coils in the PVPh/P4VP mixture are well separated in DMF solutions; therefore, the polymer chains are rather extended prior to solvent evaporation because the interassociation hydrogen bonding between PVPh and DMF is stronger than that between PVPh and P4VP.[38,42] As a result, the stronger hydrogen bonding between PVPh and P4VP in MeOH tends to induce polymer complex aggregation. In previous studies,[43−46] we observed, from transmission electron microscopy (TEM) analyses, distinct chain behavior—separated coils and chain aggregates—also from mixtures of poly(styrene-b-vinylphenol) (PS-b-PVPh) and poly(4-vinylpyridine-b-methyl methacrylate) (P4VP-b-PMMA) in different polar solvents as a result of their ability to self-assemble into well-defined nanostructures.

In this present study, we suspected that PTyr, with its OH groups, would be another model polymer that might exhibit separated coil/aggregated chain behavior in polymer blend systems because this polypeptide can form well-defined secondary structures (α-helices, β-sheets). In addition, we expected these well-defined secondary structures to be different in the separated coils and the aggregated chains when blended with P4VP in different common solvents. Here, we used differential scanning calorimetry (DSC), Fourier transform infrared (FTIR) spectroscopy, solid state nuclear magnetic resonance (NMR) spectroscopy, and wide-angle X-ray diffraction (WAXD) to investigate the miscibility behavior, hydrogen bonding interactions, and secondary structures of PTyr/P4VP blends and their corresponding complexes.

■ EXPERIMENTAL SECTION

Materials. ʟ-Tyrosine was purchased from MP Biomedicals. Triphosgene (TCI), propargylamine (Acros, 99%), P4VP (Aldrich, 60 000 Da), DMF (Echo, 99.5%), MeCN (Acros, 99.5%), hexane (Acros), MeOH (Acros), tetrahydrofuran (THF, Tedia) were purchased commercially. All reaction mixtures were magnetically stirred under Ar. Solvents were distilled from an appropriate drying agent prior to use.

ʟ-Tyrosine *N*-carboxyanhydride (Tyr-NCA).[47] Triphosgene (5.30 g, 17.7 mmol) was added to a solution of ʟ-tyrosine (8.00 g, 44.2 mmol) in MeCN (300 mL) heated under reflux (70 °C) under a N₂ atmosphere. After continuing refluxing for 4 h, the solution cooled to 0 °C. The solvent was removed through rotary evaporation and the

product recrystallized three times from THF/hexane. Yield: 5.6 g, 27.1 mmol, 61.3%. ¹H NMR (DMSO): δ (ppm) = 2.90 (d) 2H, CH₂), 4.69 (t, 1H), 6.69 (d, 2H, Ar), 6.95 (d, 2H, Ar), 9.02 (s, 1H), 9.33 (s, 1H, NH). FTIR (KBr, cm⁻¹): 3313 (NH), 1846 (C=O), 1762 (C=O), 1601 (OH), 1590, 753, 698 (Ar).

Propargyl-Terminated Poly-ʟ-Tyrosine (PTyr). Tyr−NCA (4.00 g, 19.3 mmol) was weighed in a drybox under N₂, placed in a three-neck bottle, and dissolved in anhydrous DMF (20 mL). The solution was stirred for 10 min and then propargylamine (0.25 mL, 96.5 mmol) was added using a N₂-purged syringe. After stirring for 2 days at 0 °C, the polymer was recovered through precipitation in Et₂O and drying under high vacuum. Table 1 lists the degree of

Table 1. Characterization of the PTyr Prepared in This Study

polymer	$M_n{}^a$	$M_n{}^b$	PDI[b]	$M_n{}^c$	PDI[c]
PTyr₈	1030	3300	1.05	1350	1.05

[a]Determined from ¹H NMR spectrum. [b]Determined from GPC analysis. [c]Determined from MADLI−TOF mass spectrum.

polymerization (DP) of PTyr used in this study, as determined using ¹H NMR spectroscopy and MALDI−TOF mass spectrometry, and the synthesis is depiced in Scheme 1. Yield: 2.5 g, 2.85 mmol, 14.8%. ¹H NMR (DMSO): δ (ppm) = 4.40 (t, 1H), 6.69 (d, 2H, Ar), 6.95 (d, 2H, Ar), 7.94 (s, 1H, NH), 9.14 (s, 1H). FTIR (KBr, cm⁻¹): 3288 (NH), 1601 (benzene), 753, 698 (Ar).

Blend Preparation. Mixtures of PTyr/P4VP at various blend compositions were prepared through solution-casting. A DMF solution containing the polymer mixture (5 wt %) was stirred for 6−8 h and then the solvent was evaporated slowly at 50 °C for 1 day. The film of the blend was then dried at 80 °C for 2 days to ensure total removal of residual solvent.

Complex Preparation. PTyr/P4VP complexes were prepared by dissolving pure PTyr and pure P4VP separately in MeOH. Each solution was stirred overnight to ensure complete dissolution. The two solutions were then mixed together to give a white precipitate, which was filtered off and washed with MeOH. The samples were then dried under vacuum to remove any residual solvent. The ratio of the content of the complex to the total amounts of the two polymers in the initial solutions was considered as the yield of the complex. The bulk compositions of the complexes were determined through elemental analyses; the results are summarized in Table 2.

Characterization. ¹H NMR spectra were recorded at room temperature using a Bruker AM 500 (500 MHz) spectrometer, with the residual proton resonance of the deuterated solvent used as the internal standard. High-resolution solid state NMR spectra were recorded at room temperature using a Bruker DSX-400 spectrometer operated at resonance frequencies of 399.53 and 100.47 MHz for ¹H and ¹³C nuclei, respectively. ¹³C cross-polarization (CP)/magic angle sample spinning (MAS) spectra were measured using a 3.9-μs 90° pulse, a 3-s pulse delay time, a 30-ms acquisition time, and 2048 scans. All NMR spectra were recorded at 300 K using broad band proton decoupling and a normal CP pulse sequence. An MAS rate of 5.4 kHz was used to avoid absorption overlapping. Mass spectra were obtained using a Bruker Daltonics Autoflex MALDI−TOF mass spectrometer. The following voltage parameters were employed: ion source 1, 19.06 kV; ion source 2, 16.61 kV; lens, 8.78 kV; reflector 1, 21.08 kV; reflector 2, 9.73 kV. Molecular weights and molecular weight distributions were determined through gel permeation chromatography (GPC) using a Waters 510 high-performance liquid chromatography (HPLC) system equipped with a 410 differential refractometer and three Ultrastyragel columns (100, 500, and 10³ Å) connected in series, with DMF as the eluent (flow rate: 0.4 mL/min). DSC was performed using a TA-Q20 instrument operated at a scan rate of 10 °C/min over the temperature range from 25 to 220 °C under a N₂ atmosphere. FTIR spectra of the polymer films were recorded using a Bruker Tensor 27 FTIR spectrophotometer and the conventional KBr disk method; 32 scans were collected at a spectral

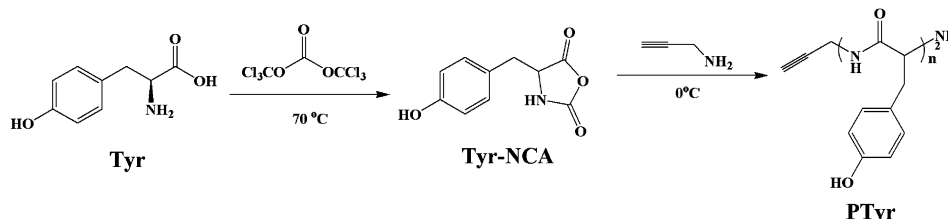**Scheme 1. Synthesis of PTyr Using Propargylamine as the Initiator**

<table>
<tr><td colspan="7" align="center">**Table 2. Characteristic and Thermal Properties of PTyr/P4VP Complexes**</td></tr>
</table>

Table 2. Characteristic and Thermal Properties of PTyr/P4VP Complexes

feed composition		bulk composition			
PTyr	P4VP	PTyr	P4VP	yield (wt %)	T_g (°C)
20	80	37	63	35	183
40	60	41	59	42	186
50	50	45	55	55	184
60	40	52	48	64	184
80	20	60	40	38	183

(header spanning: PTyr/P4VP)

resolution of 1 cm⁻¹. Because polymers containing OH groups are hygroscopic, pure N_2 gas was used to purge the spectrometer's optical box to ensure dry sample films. X-ray diffraction (XRD) data were collected on the wiggler beamline BL17A1 of the National Synchrotron Radiation Research Center (NSRRC), Taiwan. A triangular bent Si (111) single crystal was employed to obtain a monochromated beam having a wavelength (λ) of 1.33001 Å. The XRD patterns were collected using an imaging plate (IP; Fuji BAS III; area = 20 × 40 cm²) curved with a radius equivalent to the sample-to-detector distance (280 mm). The two-dimensional (2D) XRD patterns of the samples (typical diameter: 10 mm; thickness: 1 mm) were circularly averaged to obtain one-dimensional (1D) diffraction profiles $I(Q)$. The values of Q were calibrated using standard samples of silver behenate and Si powder (NBS 640b).

■ RESULTS AND DISCUSSION

Synthesis of PTyr. Figure 1 displays FTIR spectra of the tyrosine monomer and corresponding polymer, recorded at room temperature. Two typical C=O stretching bands—at

1837 and 1765 cm⁻¹, corresponding to the C=O units a and b, respectively—confirm the formation of the NCA ring.[48] After ring-opening polymerization of the NCA monomer, the FTIR spectrum revealed the absence of the absorbances from the C=O groups a and b of the NCA ring and the appearance of new signals at 1655, 1630 (c), and 1545 (d) cm⁻¹ representing the amide bonds in the polymer backbone.[48]

Figure 2a presents the ¹H NMR spectrum of the tyrosine monomer in d_6-DMSO. We assign the singlet at 9.34 ppm to the proton on the nitrogen atom, the signal at 9.04 ppm to the proton of the phenolic OH group, the doublets at 6.97 and 6.66 ppm to the protons of the benzyl ring, and the triplet at 4.66 and doublet at 2.49 ppm to the alkyl CH_2 and CH protons. Figure 2b displays the ¹H NMR spectrum of PTyr in d_6-DMSO. The signal of the protons on the nitrogen atoms of PTyr appeared at 8.05 ppm (singlet); the signal of the phenolic OH proton appeared at 9.24 ppm; the singlets at 2.30 and 3.83 ppm correspond to the C≡C−H and C≡CCH₂ protons, respectively; and the signals of the aromatic protons appeared as 6.97 and 6.66 ppm. Figure 2 provides assignments for all of the other signals in the ¹H NMR spectrum of PTyr. We determined the molar mass of PTyr from its ¹H NMR spectrum using the equation[49,50]

$$M_{n,PTyr} = \frac{I_e M_{Tyr}}{2I_g} + M_{propargylamine}$$

where I_e and I_g are the intensities of the signals of the methine protons e on the main chain of PTyr and the methylene protons g of the propargylamine initiator, respectively, and $M_{propargylamine}$ is the molar mass of the propargylamine initiator.
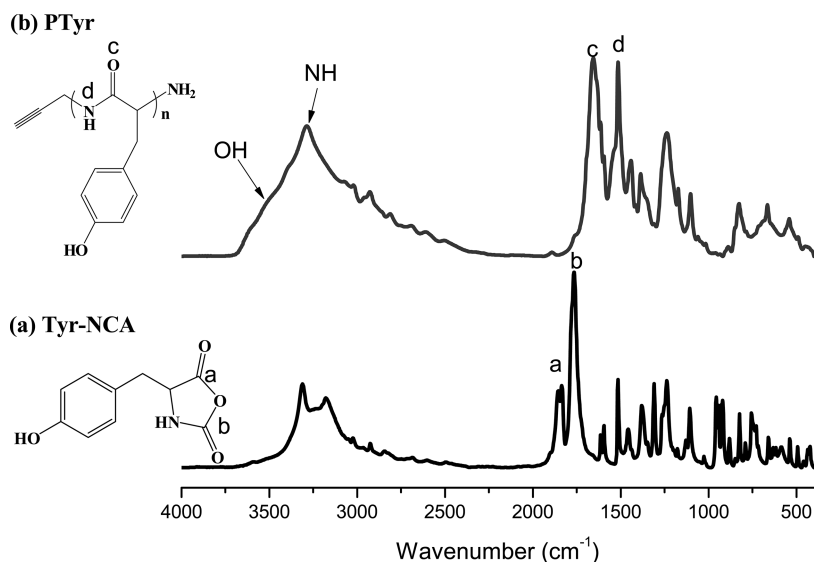

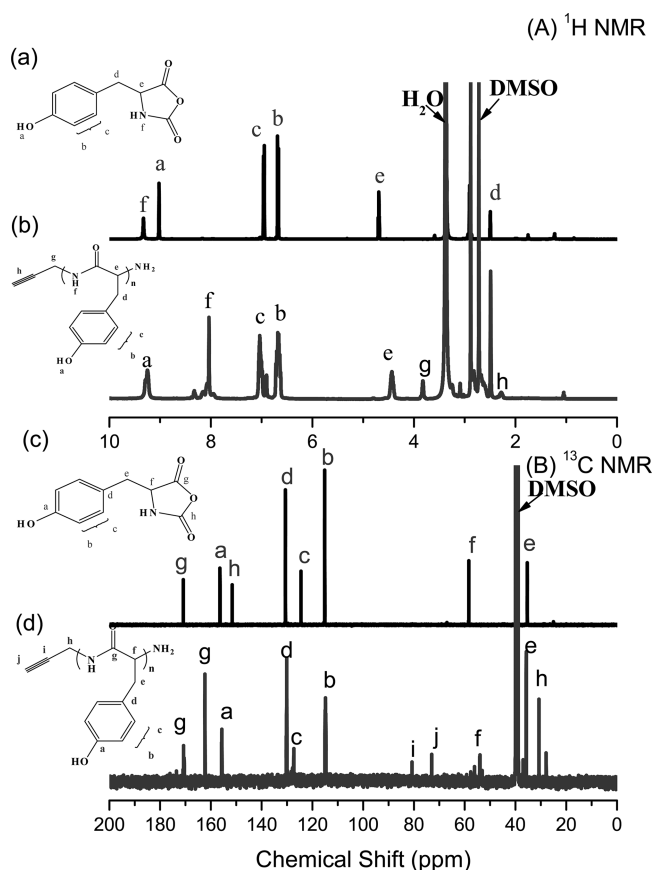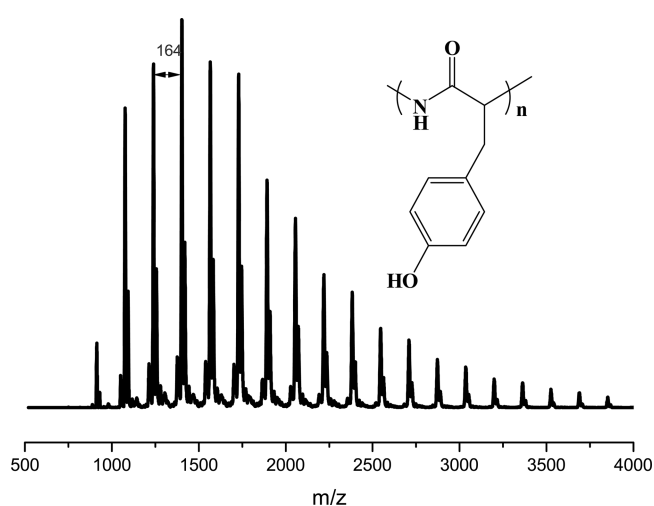**Figure 1.** FTIR spectra of the (a) tyrosine NCA monomer and (b) PTyr polypeptide at room temperature.

(A) ^{1}H NMR

**Figure 2.** (A) ^{1}H and (B) ^{13}C NMR spectra of the (a, c) tyrosine NCA monomer and (b, d) PTyr polypeptide.


Figure 3. MALDI−TOF mass spectrum of the PTyr polypeptide.

Here, we chose propargylamine as the macroinitiator because it provided the potential ability to synthesize block copolymers using click reactions[18,19] (for brevity, we will discuss such materials in a future paper).

Figure 2c presents the ^{13}C NMR spectrum of the tyrosine monomer in d_6-DMSO. The signals for the C=O carbon atoms appear at 171.2 and 151.2 ppm; the signal for the phenolic C−OH carbon atom appears at 156.6 ppm; those of the phenyl ring appear at 130.3, 124.4, and 114.8 ppm. The signals for the benzylic carbon atom and the amino acid α-
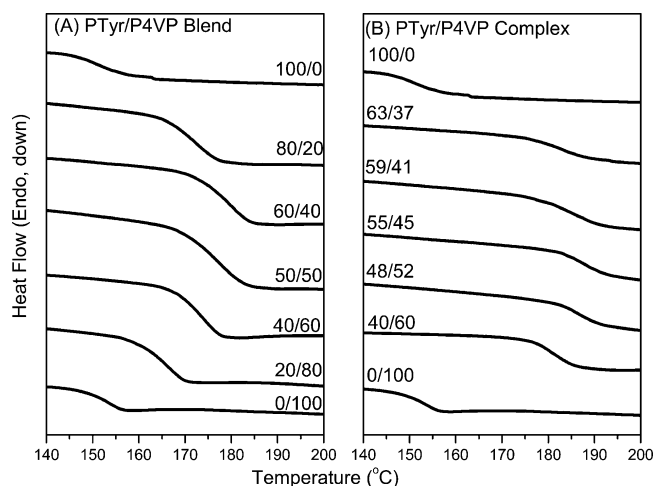

Figure 4. DSC traces (second heating run) of (A) PTyr/P4VP blends and (B) PTyr/P4VP complexes.
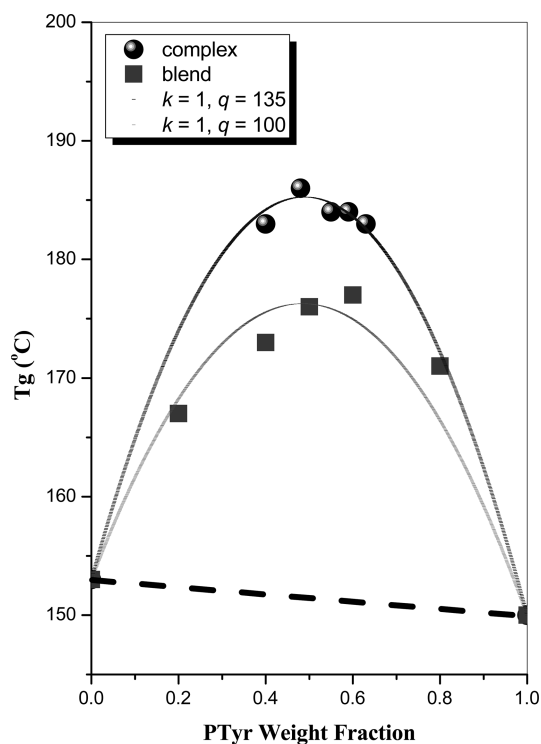
Figure 5. Plots of T_g with respect to composition, based on the Kwei equation, for PTyr/P4VP blends and complexes.

carbon atom (NHCO**C**) appear at 34.7 and 58.2 ppm, respectively. Figure 2d displays the ^{13}C NMR spectrum of PTyr in d_6-DMSO; the signals for the amide carbon atoms appear at 170 and 162 ppm, while those of the alkyne carbon atoms (derived from the macroinitiator propargylamine) appear at 72 and 80 ppm. The signals for the amino acid α-carbon atoms (NHCO**C**) appear at 54.3 ppm. Figure 2(d) provides assignments for the remaining signals of the carbon atoms of PTyr. Figure 3 presents the MALDI−TOF mass spectrum of PTyr. The mass difference between all adjacent peaks for PTyr is m/z 164, as expected for a tyrosine repeating unit. Taken together, the ^{1}H NMR, ^{13}C NMR, FTIR, and MALDI−TOF mass spectra confirmed the successful synthesis
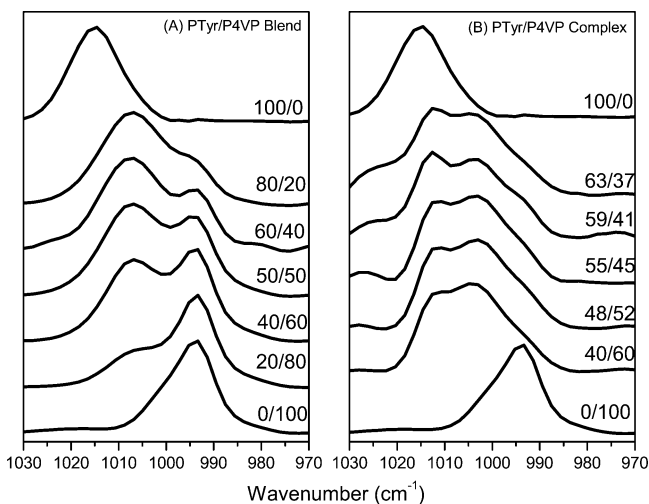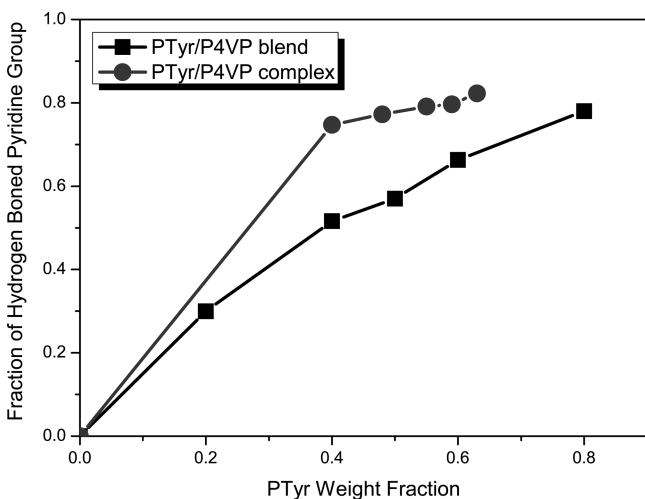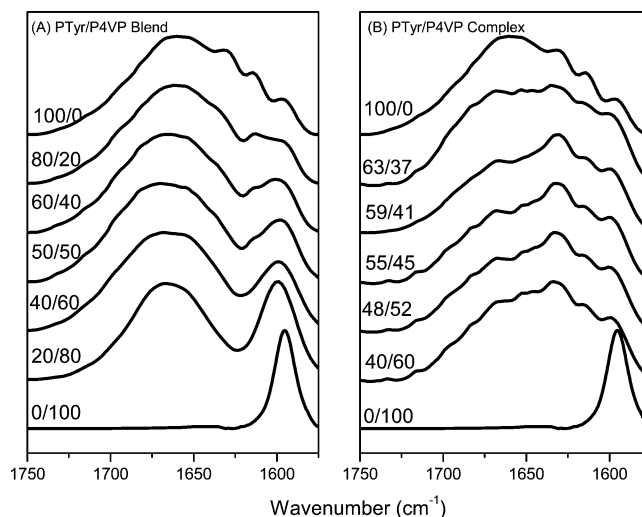
Figure 6. IR spectra, recorded at room temperature, displaying the region between 1030 and 970 cm^{-1}, for (A) PTyr/P4VP blends and (B) PTyr/P4VP complexes.

Table 3. Fractions of Hydrogen-Bonded Components in PTyr/P4VP Blends and Complexes at Room Temperature, Determined from Curve Fitting of FTIR Spectral Data

	free pyridyl rings			hydrogen-bonded pyridyl rings			
blend	ν, cm^{-1}	$W_{1/2}$, cm^{-1}	A_f, %	ν, cm^{-1}	$W_{1/2}$, cm^{-1}	A_b, %	f_b, %
20/80	993	10	70.0	1005	11	30.0	30.0
40/60	993	10	48.4	1005	11	51.6	51.6
50/50	994	10	43.0	1006	11	57.0	57.0
60/40	994	9	33.7	1006	11	66.3	66.3
80/20	994	9	22.0	1006	12	78.0	78.0
Complex							
40/60	993	8	25.3	1003	11	74.7	74.7
48/52	993	8	22.8	1003	11	77.2	77.2
55/45	994	8	20.9	1003	11	79.1	79.1
59/61	994	8	20.4	1003	11	79.6	79.6
63/37	994	8	17.8	1004	11	82.2	82.2

Figure 7. Fraction of pyridyl groups of P4VP hydrogen bonded to the polypeptide, plotted with respect to the PTyr content in the blend and complex systems.
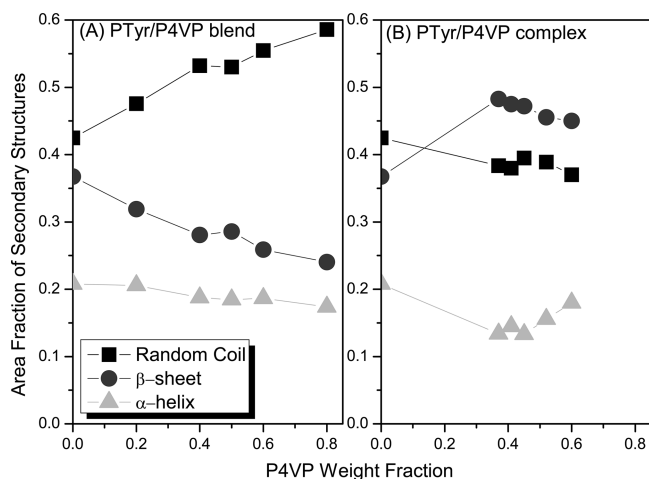

Figure 8. FTIR spectra (1750−1580 cm^{-1}) recorded at room temperature of (A) PTyr/P4VP blends and (B) PTyr/P4VP complexes.
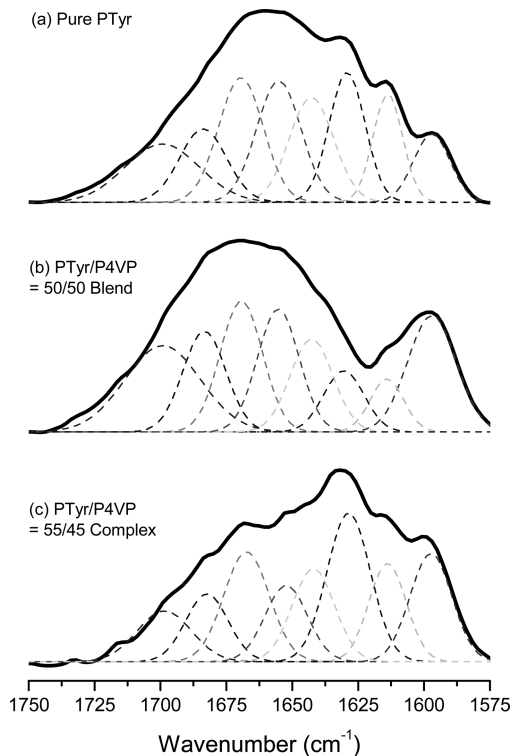

Figure 9. Curve fitting of the signals in the FTIR spectra of (a) pure PTyr, (b) the PTyr/P4VP =50/50 blend, and (c) the PTyr/P4VP = 55/45 complex.

of PTyr. Table 1 lists the DP of PTyr used in this study, as determined from its ^{1}H NMR and MALDI−TOF mass spectra.

Thermal Analyses of PTyr/P4VP Blends and Complexes. Generally, only a single glass transition can be observed if the components of blends and complexes are thermodynamically miscible. DSC is a convenient method for observing the thermal characteristics that arise from the different interactions of miscible polymer blends and complexes. Here, we increased the feed composition up to the bulk composition, similar to the method reported for poly(methacrylic acid) (PMAA)/P4VP complex systems.[51] The

Figure 10. Secondary structures in the (A) PTyr/P4VP blends and (B) PTyr/P4VP complexes at various P4VP contents.
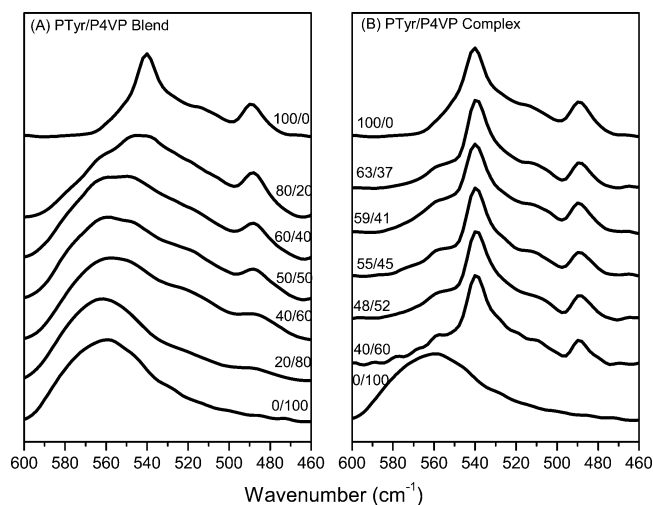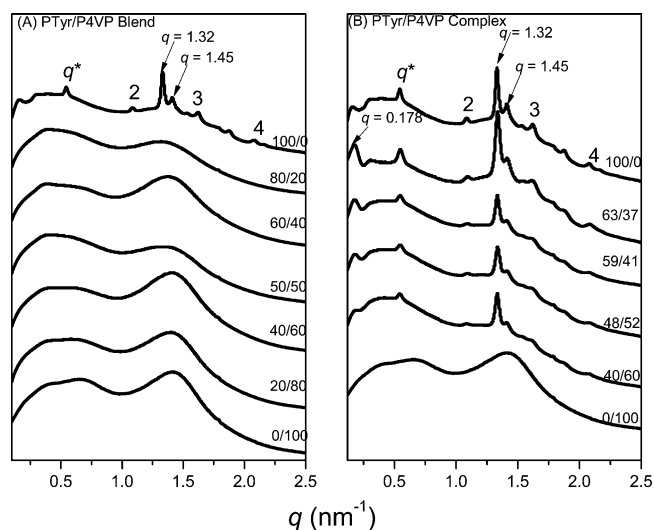

Figure 11. FTIR spectra (600−460 cm^{-1}) recorded at room temperature for the (A) PTyr/P4VP blends and (B) PTyr/P4VP complexes.
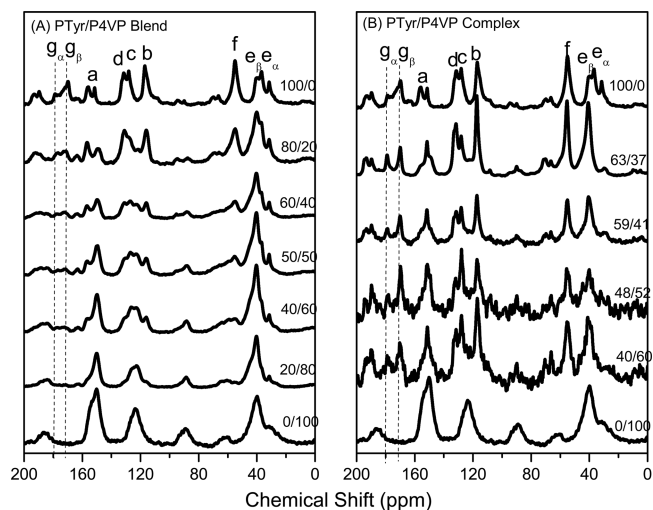
Figure 12. ^{13}C CPMAS spectra (recorded at room temperature) for the (A) PTyr/P4VP blends and (B) PTyr/P4VP complexes.


Figure 13. WAXD patterns of the (A) PTyr/P4VP blends and (B) PTyr/P4VP complexes.

DSC thermograms of various PTyr/P4VP blends and complexes in Figure 4 reveal that all of the blends and complexes exhibited only a single glass transition, suggesting that these PTyr/P4VP blends and complexes were fully miscible with a homogeneous amorphous phase. Meanwhile, we observed a single value of T_g that was higher than that of either individual polymer. A large positive deviation in the value of T_g indicates a strong interaction between the two components. This result is similar to the glass transition behavior of PVPh/P4VP miscible blend systems obtained from DMF solutions. The T_g composition curves of the miscible blends and complexes in Figure 5 reveal that the single values of T_g of all blends and complexes were significantly higher than those predicted by the Fox or linear rule. Generally, if the T_g−composition relationship deviates substantially, neither the linear relationship nor the ideal Fox rule is applicable.[52] In general, the Kwei equation[53] is a more appropriate fit to the T_g−composition relationship for highly deviated miscible block copolymer or polymer blends:

$$T_g = \frac{W_1 T_{g1} + k W_2 T_{g2}}{W_1 + k W_2} + q W_1 W_2 \tag{2}$$

where w_1 and w_2 are the weight fractions of the compositions, T_{g1} and T_{g2} are the corresponding glass transition temperatures, and k and q are fitting constants. Figure 5 displays the dependence of the value of T_g on the composition of the miscible blends and complexes of PTyr/P4VP, where the maximum deviations of the highest value of T_g were obtained when the blend compositions were PTyr/P4VP = 50/50−60/40. In this study, we obtained values of k and q of 1 and 135, respectively, for the complex and 1 and 100, respectively, for the blends, determined from the nonlinear least-squares best fits in Figure 5. Here, q is a parameter corresponding to the strength of hydrogen bonding in the system; it reflects a balance between the breaking of self-association hydrogen bonds and the forming of interassociation hydrogen bonds. Furthermore, the observed difference in the value of q from these two systems implies that the strength of the interassociation interaction within the PTyr/P4VP complex was greater than that in the corresponding PTyr/P4VP blend, consistent with our previous findings.[38] It is generally believed

Scheme 2. Possible Structures of (a) pure PTyr and (b) PTyr/P4VP Complexes
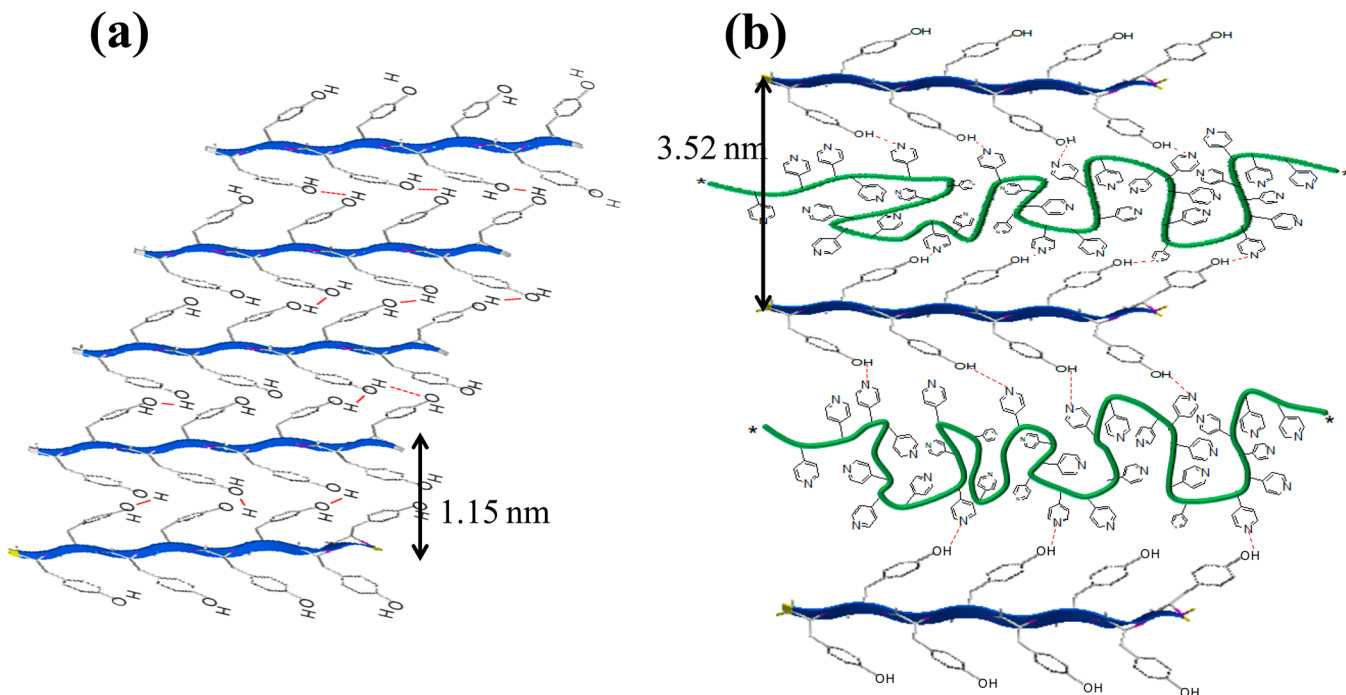
Scheme 3. Possible Structures for the Polymer Chains in the (a) PTyr/P4VP Blends and (b) PTyr/P4VP Complexes
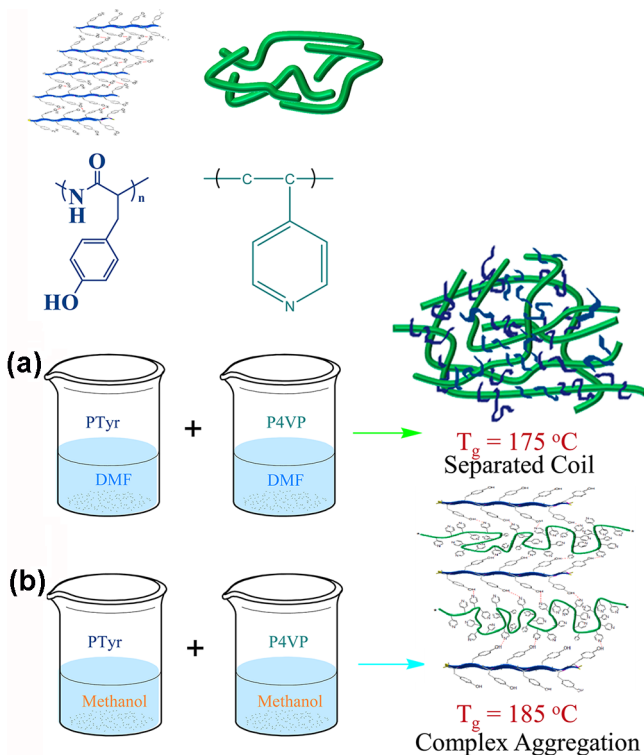
that interassociation between two polymer chains in a complex reduces segmental mobility, thereby increasing their glass transition temperatures. In addition, the positive value of q of 100 obtained for the PTyr/P4VP blend is similar to that for PVPh/P4VP blends obtained from DMF solution.[38]

FTIR Spectroscopic Analyses of PTyr/P4VP Blends and Complexes. FTIR spectroscopy can provide information

about specific interactions between polymers and the secondary structures of polypeptides, both qualitatively and quantitatively.[54,55] Some of the characteristic modes of P4VP are sensitive to the presence of hydrogen bonds, and have been widely discussed. For example, the signals of P4VP at 1590, 1050, 993, and 625 cm^{-1} shifted to 1600, 1067, 1011, and 634 cm^{-1}, respectively, after hydrogen bonding with the carboxylic acid groups of poly(ethylene-co-methacrylic acid).[56] Unfortunately, it was difficult for us to analyze the band at 1590 cm^{-1} for P4VP because of overlap with the band at 1600 cm^{-1} from PTyr. Indeed, we could use only the band at 993 cm^{-1} to analyze the hydrogen bonding interactions between the OH groups of PTyr and the pyridyl groups of P4VP. Figure 6 presents room-temperature FTIR spectra in the range 970–1030 cm^{-1} for the PTyr/P4VP blends and complex. Pure P4VP provided a characteristic band at 993 cm^{-1}, corresponding to the free pyridyl rings; pure PTyr provided a band at 1015 cm^{-1}. These two bands were well resolved, without overlapping. A new band appeared at 1003–1006 cm^{-1}, which we assign to the hydrogen-bonded pyridyl rings of P4VP in the PTyr/P4VP blends and complexes. The FTIR spectra of all of the blend and complex systems revealed the existence of hydrogen bonding between the pyridyl and OH groups, but it was difficult to quantify the degree of hydrogen bonding because of the presence of three bands in this region. As a result, we performed a digital subtraction of the signal for pure PTyr at 1015 cm^{-1}, based on the weight fraction of P4VP in these blends and complexes.[38,57] All of the signals for the pyridyl groups split into two bands that fit well to the Gaussian function (Table 3). Figure 7 summarizes the results from curve fitting; the fraction of hydrogen-bonded pyridyl rings increased upon increasing the PTyr content in the blend and complex systems, similar to our previously reported findings for phenolic/P4VP and PVPh/P4VP blends.[38,56] In addition, the fraction of hydrogen-bonded pyridyl groups of P4VP at the same PTyr weight fraction revealed that the degree of hydrogen bonding in the complex was greater than that of the blends;

these results are consistent with those determined using the Kwei equation.

Figure 8 presents FTIR spectra recorded at room temperature in the range from 1750 to 1580 cm^{-1}, providing information regarding the secondary structures (amide I group) of the PTyr/P4VP blends and complexes. Analyzing these spectra using the second-derivative technique,[7] we observed eight major peaks for pure PTyr: for the ring vibrations of tyrosine at 1597 and 1615 cm^{-1}; the α-helical conformation at 1655 cm^{-1}; the β-sheet conformation at 1630 cm^{-1}; the β-turn conformation at 1670 cm^{-1}; and the random coil conformation at 1643, 1683, and 1700 cm^{-1}.[58] After blending with the P4VP homopolymer, the fraction of the β-sheet conformation at 1630 cm^{-1} increased initially at lower P4VP homopolymer contents but then decreased at higher P4VP homopolymer contents in the complex system. For deconvolution, we fitted a series of Gaussian distributions (Figure 9) to quantify the fractions of each of the peaks. Figure 10 summarizes the curve-fitting data for the amide I groups of the β-sheet, α-helical, and random coil structures of PTyr when blended and complexed with the P4VP homopolymer. It has been reported that the α-helix and β-sheet secondary structures of PBLG are both present at low DPs (<18), but when the DP increases, the α-helical secondary structure is favored.[28] In this study, we also observed both the α-helix and β-sheet conformations for the PTyr oligomer at a DP of 8. When blended with the P4VP, the fractions of the α-helix and β-sheet conformations decreased, implying that the fraction of random coil conformations increased, upon increasing the content of the P4VP homopolymer. When complexed with P4VP, which can form strong hydrogen bonds, the fractions of the random coil and α-helix conformations were lower than that of pure PTyr, implying that the fraction of β-sheet conformations was higher than that in pure PTyr. Therefore, the secondary structures for PTyr were highly dependent on the strength of the intermolecular interactions and the chain behavior in solution.

In addition to amide I bands, amide VI bands are also sensitive to secondary structure modifications of polypeptides. The relative contributions of α-helix and β-sheet conformations are well correlated with the absorptions of the amide I bands. Unfortunately, our analysis of the random coil structures were difficult because the three major peaks contributing to the amide I bands of the tyrosine residues in the random coil conformation were strongly overlapped with the signals for the ring vibrations (1597 and 1615 cm^{-1}) of the α-helix and β-sheet conformations.[58] Figure 11 presents FTIR spectra recorded at room temperature in the range from 600 to 460 cm^{-1}, from which we obtained information regarding the secondary structures (amide VI group) of the PTyr/P4VP blends and complexes. We attribute the signal near 540 cm^{-1} to a predominant β-sheet conformation and that at 512 cm^{-1} to an α-helical conformation.[58] The fraction of β-sheet conformations decreased significantly upon increasing the P4VP content in the PTyr/P4VP blend system; in contrast, the fraction of β-sheet conformations remained almost unchanged upon increasing the P4VP content in the PTyr/P4VP complex system, consistent with our findings from analyses of the signals for the amide I groups.

The solvent medium can play an important role in affecting or controlling the type of complex that forms.[39] PTyr/P4VP yielded a complex precipitate in MeOH, but no precipitation occurred in DMF. Because solvent molecules can also participate in hydrogen bonding interactions, they can compete with P4VP for the OH groups in PTyr. MeOH is a relatively weaker hydrogen bond acceptor than DMF. As a result, the PTyr/P4VP blends also formed interpolymer complexes in MeOH, but not in DMF, a solvent that has a great ability to break hydrogen bonds.[39−41] Furthermore, the values of T_g of the PTyr/P4VP complexes obtained from MeOH solutions were always higher than those of the miscible PTyr/P4VP blends obtained from DMF solution casting. The random coils were well separated for the PTyr/P4VP mixture in DMF solution, with the polymer chains being quite extended prior to solvent evaporation because interassociation hydrogen bonding between PTyr and DMF was stronger than that between PTyr and P4VP. As a result, the random coil conformation was preferred in the PTyr/P4VP blend systems. In contrast, the stronger hydrogen bonding between PTyr and P4VP in MeOH tended to induce polymer complex aggregation, with a possible mechanism involving the formation of interpolymer complexes through interchain hydrogen bonding of two polymer chains. As a result, the content of β-sheets stabilized through intermolecular interactions increased in the PTyr/P4VP complex systems. To confirm this hypothesis, we explored the secondary structures using solid state NMR spectroscopy and WAXD.

Solid State NMR Spectroscopic and WAXD Analyses of PTyr/P4VP Blends and Complexes. Figure 12 displays ^{13}C CP/MAS spectra of the PTyr/P4VP blends and complexes at room temperature. The different ^{13}C chemical shifts of the C_α, C_β, and amide C=O carbon atom nuclei were related to the different local conformations of the individual amino acid residues, characterized by their dihedral angles and types of intermolecular and intramolecular hydrogen bonds.[59,60] In the case of pure PTyr, the phenolic groups in the side chains could stabilize the α-helical secondary structures; the chemical shifts of the corresponding C_α, C_β, and amide C=O carbon atom nuclei appeared at 58.0, 36.1, and 177.0 ppm, respectively. In the β-sheet conformation, these chemical shifts (52.1, 39.3, and 169.6 ppm, respectively) were located upfield by approximately 3−7 ppm relative to those for the α-helical conformations.[60] Other assignable signals were similar to those in Figure 2d. The C=O region of the spectrum of the PTyr/P4VP blend system revealed that the contents of the α-helical and β-sheet conformations of PTyr disappeared gradually upon increasing the P4VP content. In contrast, the fraction of β-sheet conformations remained almost unchanged upon increasing the P4VP content in the PTyr/P4VP complex system, similar to our findings from analyses of the amide VI bands using FTIR spectroscopy.

We also used WAXD to identify the changes in the secondary structures of the PTyr/P4VP blends and complexes (Figure 13). For pure PTyr at a DP of 8, the diffraction pattern revealed the presence of β-sheet secondary structures. The first peak, at a value of q of 0.54, reflects the distance ($d = 1.15$ nm) between the backbones in the antiparallel β-pleated sheet structure; the high-order diffraction maxima at scattering vectors q of multiple integers relative to the position of the first-order scattering maximum ($q/q_m = 1, 2, 3,$ and 4) also suggested that the PTyr featured a lamellar microdomain structure. The reflection at a value of q of 1.32 ($d = 0.475$ nm) represents the intermolecular distance between adjacent peptide chains within one lamella; the value of q of 1.45 originated mainly from the repeated residues of the polypeptide chain ($d = 0.445$ nm).[61] The features in the X-ray patterns

gradually become a broad amorphous halo arising from the random coil conformations upon increasing the P4VP content in the PTyr/P4VP blend system, consistent with our FTIR and solid state NMR spectroscopic analyses. In contrast, the signals in the X-ray pattern at values of q of 0.54 and 1.32 remained almost unchanged upon increasing the P4VP content in the PTyr/P4VP complex system, indicating that the PTyr maintained its β-pleated sheet structure. We expected that the interactions of the P4VP homopolymer through hydrogen bonding at the PTyr side chains should have expanded or swollen the distance between the β-pleated sheets in the PTyr/P4VP complex. Figure 13(B) reveals that the WAXD pattern of the PTyr/P4VP complexes featured more than one strong additional diffraction angle (at $q = 0.178$) relative to that of pure PTyr. This broad peak, assumed to be a Bragg reflection, corresponds to an ordered spacing of approximately 3.52 nm for the PTyr/P4VP complexes. Increasing the P4VP homopolymer content did not change the position of this diffraction peak. Scheme 2 provides a schematic representation of the organization of the β-pleated sheet structures for PTyr and the PTyr/P4VP complex. As calculated from the WAXD data, the β-pleated sheet lamellar structure for PTyr has a separation of 1.15 nm (Scheme 2a); the characteristic spacing of 3.52 nm in Scheme 2b is consistent with a β-pleated sheet lamellar structure with random coils of P4VP homopolymer chains.

Scheme 3 summarizes the possible morphologies, secondary structures, and intermolecular interactions in the PTyr/P4VP blends and complexes. The α-helical and β-sheet conformations are stabilized by intra- and intermolecular hydrogen bonding interactions, respectively. Upon blending with P4VP in DMF solution, random coils of PTyr were well separated and the polymer chains were quite extended prior to solvent evaporation; FTIR spectra, solid state NMR spectra, and WAXD analyses revealed that the PTyr/P4VP blend featured a random coil conformation after solvent evaporation (Scheme 3a). The higher value of T_g for the PTyr/P4VP complex relative to those for the PTyr/P4VP blends was probably due to interpolymer complex aggregation through intermolecular hydrogen bonding interactions, which stabilized the β-sheet conformations (Scheme 3b).

CONCLUSIONS

We have successfully synthesized a low-molecular-weight PTyr through living ring-opening polymerization of the corresponding α-amino acid-N-carboxyanhydride. DSC analyses revealed higher glass transition temperatures for the PTyr/P4VP complexes relative to their corresponding PTyr/P4VP blends, as a result of stronger intermolecular hydrogen bonding. FTIR spectra provided evidence for specific interactions in the PTyr/P4VP blends and complexes, arising from hydrogen bonds between the OH groups of PTyr and the pyridyl groups of P4VP. The higher values of T_g for the PTyr/P4VP complex relative to those for the PTyr/P4VP blends was probably due to interpolymer complex aggregation in the MeOH solution. The well-defined β-sheet secondary structure in the PTyr/P4VP complex was rigid relative to the random coil conformation in the PTyr/P4VP blend systems (as determined from FTIR spectra, solid state NMR spectra, and WAXD analyses), resulting in higher values of T_g. Taken together, this system appears to be another suitable model for identifying the behavior of separated coils and aggregated chains in polymer blend and complex systems.

AUTHOR INFORMATION

Corresponding Author
*E-mail: kuosw@faculty.nsysu.edu.tw. Telephone/Fax: 886-7-5254099.

Notes
The authors declare no competing financial interest.

REFERENCES

(1) Meyer, D. E.; Chilkoti, A. *Biomacromolecules* **2002**, *3*, 357.
(2) Deming, T. J. *Adv. Mater.* **1997**, *9*, 299.
(3) Yu, M.; Nowak, A. P.; Deming, T. J. *J. Am. Chem. Soc.* **1999**, *121*, 12210.
(4) Engler, A. C.; Lee, H.; Hammond, P. T. *Angew. Chem., Int. Ed.* **2009**, *48*, 9334.
(5) Chen, Y.; He, C.; Xiao, C.; Ding, J.; Zhuang, X.; Chen, X. *Polym. Chem.* **2011**, *2*, 2627.
(6) Zhou, C.; Leng, B.; Yao, J.; Qian, J.; Chen, X.; Zhou, P.; Knight, D. P.; Shao, Z. Z. *Biomacromolecules* **2006**, *7*, 2415.
(7) Sanchez-Ferrer, A.; Mezzenga, R. *Macromolecules* **2010**, *43*, 1093.
(8) Zhou, Q. H.; Zheng, J. K.; Shen, Z. H.; Fan, X, H.; Chen, X. F.; Zhou, Q. F. *Macromolecules* **2010**, *43*, 5367.
(9) Lee, H. F.; Sheu, H. S.; Jeng, U. S.; Huang, C. F.; Chang, F. C. *Macromolecules* **2005**, *38*, 6551.
(10) Papadopoulos, P.; Floudas, G.; Schnell, I.; Aliferis, T.; Iatrou, H.; Hadjichristidis, N. *Biomacromolecules* **2005**, *6*, 2352.
(11) Rao, J.; Zhang, Y.; Zhang, J.; Liu, S. *Biomacromolecules* **2008**, *9*, 2586.
(12) Klok, H. A.; Langenwalter, J. F.; Lecommandoux, S. *Macromolecules* **2000**, *33*, 7819.
(13) Lecommandoux, S.; Achard, M. F.; Langenwalter, J. F.; Klok, H. A. *Macromolecules* **2001**, *34*, 9100.
(14) Crespo, J. S.; Lecommandoux, S.; Borsali, R.; Klok, H. A.; Soldi, V. *Macromolecules* **2003**, *36*, 1253.
(15) Papadopoulos, P.; Floudas, G.; Schnell, I.; Lieberwirth, I.; Nguyen, T. Q.; Klok, H. A. *Biomacromolecules* **2006**, *7*, 618.
(16) Klok, H. A.; Lecommandoux, S. *Adv. Polym. Sci.* **2006**, *202*, 75.
(17) Kuo, S. W.; Lee, H. F.; Huang, W. J.; Jeong, K. U.; Chang, F. C. *Macromolecules* **2009**, *42*, 1619.
(18) Kuo, S. W.; Tsai, H. T. *Polymer* **2010**, *51*, 5605.
(19) Lin, Y. C.; Kuo, S. W. *J. Polym. Sci., Polym. Chem.* **2011**, *49*, 2127.
(20) Lin, Y. C.; Kuo, S. W. *Polym. Chem.* **2012**, *3*, 162.
(21) Lin, Y. C.; Kuo, S. W. *Polym. Chem.* **2012**, *3*, 882.
(22) Painter, P. C.; Tang, W. L.; Graf, J. F.; Thomson, B.; Colema, M. M. *Macromolecules* **1991**, *24*, 3929.
(23) Asano, A.; Kurotu, T. *J. Mol. Struct.* **1998**, *441*, 129.
(24) Murata, K.; Katoh, E.; Kuroki, S.; Ando, I. *J. Mol. Struct.* **2004**, *689*, 223.
(25) Deng, X.; Hao, J.; Yuan, M.; Xiong, C.; Zhao, S. *Polym. Int.* **2001**, *50*, 37.
(26) Aoi, K.; Nakamura, R.; Okada, M. *Macromol. Chem. Phys.* **2000**, *201*, 1059.
(27) Lu, C.; Pelton, R. *Langmuir* **2004**, *20*, 3962.
(28) Papadopoulous, P.; Floudas, G.; Klok, H. A.; Schnell, I.; Pakula, T. *Biomacromolecules* **2004**, *5*, 81.
(29) Blondelle, S. E.; Forood, B.; Houghten, R. A.; Perez-Paya, E. *Biochemistry* **1997**, *36*, 8393.
(30) Gitsas, A.; Floudas, G.; Mondeshki, M.; Spiess, H. W.; Aliferis, T.; Iatrou, H.; Hadjichristidis, N. *Macromolecules* **2008**, *41*, 8072.
(31) Kuo, S. W.; Chen, C. J. *Macromolecules* **2011**, *44*, 7315.
(32) Kuo, S. W.; Chen, C. J. *Macromolecules* **2012**, *45*, 2442.
(33) de Mefathi, M. V.; Frechet, J. M. J. *Polymer* **1988**, *29*, 477.

(34) Dai, J.; Goh, S. H.; Lee, S. Y.; Siow, K. S. *Polym. J.* **1994**, *26*, 905.

(35) Wang, J.; Cheung, M. K.; Mi, Y. *Polymer* **2001**, *42*, 3087.

(36) Xiang, M.; Jiang, M.; Zhang, Y.; Wu, C. *Macromolecules* **1997**, *30*, 2313.

(37) Zhang, Y.; Xiang, M.; Jiang, M.; Wu, C. *Macromolecules* **1997**, *30*, 6084.

(38) Kuo, S. W.; Tung, P. H.; Chang, F. C. *Macromolecules* **2006**, *39*, 9388.

(39) Wang, L. F.; Pearce, E. M.; Kwei, T. K. *J. Polym. Sci., Polym. Phys. Ed.* **1991**, *29*, 619.

(40) Dai, J.; Goh, S. H.; Lee, S. Y.; Siow, K. S. *Polym. J.* **1994**, *26*, 905.

(41) Jiang, M.; Li, M.; Xiang, M.; Zhou, H. *Adv. Polym. Sci.* **1999**, *146*, 121.

(42) Kuo, S. W. *J. Polym. Res.* **2008**, *15*, 459.

(43) Kuo, S. W.; Tung, P. H.; Lai, C. L.; Jeong, K. U.; Chang, F. C. *Macromol. Rapid Commun.* **2008**, *29*, 229.

(44) Hsu, C. H.; Kuo, S. W.; Chen, J. K.; Ko, F. H.; Liao, C. S.; Chang, F. C. *Langmuir* **2008**, *24*, 7727.

(45) Kuo, S. W.; Tung, P. H.; Chang, F. C. *Eur. Polym. J.* **2009**, *45*, 1924.

(46) Kuo, S. W. *Polym. Int.* **2009**, *58*, 455.

(47) Scheule, R. K.; Cardinaux, F.; Taylor, G. T.; Scheraga, H. A. *Macromolecules* **1976**, *9*, 23.

(48) Xiao, C.; Zhao, C.; He, P.; Tang, Z.; Chen, X.; Jing, X. *Macromol. Rapid Commun.* **2010**, *31*, 991.

(49) Agut, W.; Taton, D.; Lecommandoux, S. *Macromolecules* **2007**, *40*, 5653.

(50) Agut, W.; Agnaou, R.; Lecommandoux, S.; Taton, D. *Macromol. Rapid Commun.* **2008**, *29*, 1147.

(51) Yi, J. Z.; Goh, S. H. *Polymer* **2001**, *42*, 9319.

(52) Fox, T. G. *J. Appl. Bull. Am. Phys. Soc.* **1956**, *1*, 123.

(53) Kwei, T. K. *J. Polym. Sci.: Polym. Lett. Ed.* **1984**, *22*, 307.

(54) Chen, X. G.; Schweitzer-Stenner, R.; Asher, S. A.; Mirkin, N. G.; Krimm, S. *J. Phys. Chem. B* **1995**, *99*, 3074.

(55) Schweitzer-Stenner, R.; Sieler, G.; Mirkin, N. G.; Krimm, S. *J. Phys. Chem. A* **1998**, *102*, 118.

(56) Lee, Y. J.; Painter, P. C.; Coleman, M. M. *Macromolecules* **1988**, *21*, 954.

(57) Kuo, S. W.; Lin, C. L.; Chang, F. C. *Polymer* **2002**, *43*, 3943.

(58) Khoury, Y. E.; Hielscher, R.; Voicescu, M.; Gross, J.; Hellwig, P. *Vibr. Spectrosc.* **2011**, *55*, 258.

(59) Murata, K.; Katoh, E.; Kuroki, S.; Ando, I. *J. Mol. Struct.* **2004**, *689*, 223.

(60) Kricheldorf, H. R.; Muller, D. *Macromolecules* **1983**, *16*, 615.

(61) Auer, H. E.; Mcknight, R. P. *Biochemistry* **1978**, *14*, 2798.